SSRG International Journal of Electrical and Electronics Engineering
ISSN: 2348-8379/ https://doi.org/10.14445/23488379/IJEEE-V13I11P113

Volume 13 Issue 11, 198-208, November 2026
© 2026 Seventh Sense Research Group®

Original Article

Design Comparative Analysis of Five-Phase Fault-Tolerant Stator Permanent Magnet Flux-Switching Motor with Single- and Double-Layer Winding Configuration for Electric Vehicle Traction Applications

Stephen Eduku[1], Godwin Eshun[2], Ebenezer Narh Odonkor[3]

[1,2,3]*Department of Electrical and Electronic Engineering, Faculty of Engineering, Takoradi Technical University, Takoradi, Ghana.*

[1]*Corresponding Author: 5103180555@stmail.ujs.edu.cn*

Received: 04 September 2026 Revised: 06 November 2026 Accepted: 17 November 2026 Published: 25 Novmeber 2026

Abstract - *The five-phase fault-tolerant Single-Layer Winding Stator PM Flux-Switching (SWSPMFS) motor and Double-Layer Winding Stator PM Flux-Switching (DWSPMFS) motor with 20/19 rotor-stator pole synergy, which have not been simultaneously designed, optimized, and compared with the same design parameters and dimensions in existing literature, leaving a research gap, have been comprehensively analyzed in this research work. This study employed a multi-optimization technique in Ansys Maxwell to identify which motor is best suited for EV traction applications based on output torque, cogging torque, torque ripple, efficiency, and fault-tolerant capability. Moreover, the SWSPMFS motor unveiled an average torque of 6.41 Nm, while that of the DWSPMFS motor exhibited an average torque of 8.35 Nm. Hence, this demonstrates a 30.27% increase in the DWSPMFS motor. Nonetheless, the torque ripple exhibited by the SWSPMFS motor is 4.98%, while that of the DWSPMFS motor is 4.03%, which demonstrates a torque ripple reduction of 19.08% in the DWSPMFS motor. Besides, it is imperative to highlight that the cogging torque generated by the SWSPMFS motor is 0.33 Nm, while that generated by the DWSPMFS motor is 0.29, which demonstrates a cogging torque reduction of 12.12% in the DWSPMFS motor. Furthermore, the efficiency obtained by the SWSPMFS motor is 92.1%, while the DWSPMFS motor exhibited an efficiency of 93.98%, which depicts an increase of 2.04% in the DWSPMFS motor. Nevertheless, it can be concluded from the results that the DWSPMFS motor is a suitable potential motor candidate for EV traction applications, with better fault-tolerant capacity compared to the SWSPMFS motor.*

Keywords - *Ansys Maxwell software, Double-Layer winding, Fault-Tolerant motor, Multi-Objective optimization, Single-Layer winding, Stator PM Flux-Switching.*

1. Introduction

Global warming, caused via the exacerbation of greenhouse gases and associated environmental pollution, is recognized as the most crucial concern in recent times, consequently motivating or prompting various countries to rapidly replace traditional gasoline or Internal Combustion Engine (ICE) vehicles with newly unveiled fuels, Electric Vehicles (EV), and Hybrid Electric Vehicles (HEV) [1]. Nevertheless, environmental and economic issues are generating an impulse or driving force to design clean and cost-efficient vehicles. Nonetheless, ICE-developed vehicles contribute significantly to global warming-related issues [2].

Meanwhile, as the exhibition of gas emission of greenhouse gases, which can exacerbation of global warming, has become a critical concern, EVs are anticipated to penetrate the general market widely or comprehensively in the forthcoming years, nonetheless the operating efficiency exhibition by the designed electrical motor utilized in EV traction plays an imperative role in terms of their overall system performance level, furthermore, flux-switching designed motors have been demonstrated to be one of the key electrical motors for EV traction applications compared to other designed motors due to their ability to meet the general design requirement of higher exhibition of torque density and power density, respectively [3].

Moreover, in recent times, EV and HEVs on doubt have been recognized to become the most key viable design solution technique or proposed remedy to fuel economy or efficiency and emission minimization in terms of transportation, meanwhile drive system designed for EV and HEV traction must exhibits some key design characteristic

This is an open access article under the CC BY-NC-ND license (http://creativecommons.org/licenses/by-nc-nd/4.0/)

which are preferred, namely, higher torque density, power density, operating efficiency and overload capacity at low operating speed, currently, the Stator PM Flux-Switching (SPMFS) motor designs have no doubt have gain significant research attention owing to its distinct structure that integrate the synergy or complementarity of PMs and armature winding configurations in the stator laminated core, making the salient rotor free of PMs and windings, hence, enhancing it robustness, besides, available literature or research unveils that the SPMFS motor designs have demonstrated an exhibition of some design merits such as higher operating torque density, operating power density, enhanced operating reliability, and associated lower operating torque ripple [4-14].

Although the SPMFS motor exhibits merits such as higher operating torque density, enhanced operating controllability, minimal vibration generation, and minimal acoustic noise generation compared to similar computing motors, the SPMFS motor nonetheless exhibits significant cogging torque, complexity in terms of flux weakening analysis, and higher current design leakage, which have been the key design focus of many scholars in the field of motor design [15].

Hence, this research aimed to design and compare SPMFS motors, namely the SWSPMFS and DWSPMFS motors, which not only minimize cogging torque but also exhibit higher electromagnetic torque, efficiency, and torque density, with better fault-tolerant capability, key design requirements for EV and HEV traction applications, and to establish the key design model or motor topology between the SWSPMFS motor and DWSPMFS motor for EV traction.

Meanwhile, the SPMFS motor unveils more design merits such as inherently sinusoidally generated back-EMF generation, enhanced demagnetization tolerant and better design torque capacity [16]. Hence, there is a need to utilize it in critical applications such as EV traction owing to its brushless AC operating capacity.

Moreover, owing to the merits, namely operating efficiency density of torque and power exhibition of permanent magnet-designed motors, hence, gaining considerably popularity in applications such as electrified means of transportation, however, compared to conventional surface Permanent Magnet (PM) designed motors and interior PM motors, the flux-switching PM motors unveils the highest potential for applications such as EV and HEV, not excluding electric ship repulsion and electric designed aircraft, which is attributed to the robustness of it rotor structure and its closed exhibition of sinusoidal generated back electromotive force with excellent heat management or dissipation capability [17]. Meanwhile, electric motors utilized in EV traction applications must exhibit key design features, namely higher operating efficiency, power density, and torque density, with higher reliability operating capacity without excluding lower cost with lightweight features, which depicts the power density measure of the motor. Since higher operating torque density generation and higher operating efficiency are unveiled to be the two key design rules established for electric motors utilized in EV traction, it is imperative to improve the torque density production with minimal cogging torque exhibition to obtain a considerable enhancement of the operating efficiency [18-24].

Furthermore, the exhibition of higher torque density generation capability and power density, respectively, in the flux-switching PM motor is largely due to the energy exhibition by the rare earth PM configuration, but not excluding the motor design structure and the winding configuration or arrangement; these key design features are established as the prerequisite in EV traction applications [25-27].

Hence, continuous and extensive research is imperative to unearth an approach and design strategy of an electric motor that unveils higher electromagnetic torque and motor operating efficiency with infinitesimal or minimal torque pulsation.

Moreover, despite the extensive and widespread utilization of flux-switching PM motor in EV traction applications due to it great merits, a current and significant research gap identified in the flux-switching PM design research field and not yet explored, is that even though Stator PM Flux-Switching Motors (SPMFS-Motor) have been analyzed separately either as a single layer winding configuration or double layer winding configuration but these aforementioned two motors winding configurations synergy specially the multi-phase motor such as five-phase motor SPMFS-motor with single and double layer winding configuration has not been simultaneously designed, optimized and extensively compared to unveil which design motor topology is suitable for EV traction.

Hence, this research work aimed to design, optimize, analyze, and comprehensively and simultaneously compare a single-layer and a double-layer winding five-phase fault-tolerant SPMFS motor to determine which design candidate or motor topology is suitable for EV traction or propulsion applications.

However, the key novelty of the proposed design topologies is not merely comparing SWSPMFS motor and DWSPMFS motor simultaneously, but rather unveiling or establishing a fair design and optimized method and extensively validating a comparison that exhibits unique selection knowledge for suitable motor topology in terms of five-phase SWSPMFS motor and DWSPMFS motor for EV traction or propulsion applications, which is a research gap identify in existing literature.

2. Materials and Methods

The motors extensively considered in this research paper are Stator Permanent Magnet Flux-Switching (SPMFS) motors configured with single- and double-layer winding designs, with the same design-selected materials and dimensions to maintain or ensure a fair design analysis. Moreover, the motor topology adopts 20 stator slots and 19 rotor poles, which is verified extensively in [10] and [28] for exhibiting a better rotor pole combination, depicting an interesting design technique, in that the stator slot and rotor pole design numbers are relatively prime; thus, with a ratio of the slot pole of Qs/Pr =20/19, and corresponding GCD (Qs, Pr) = 1, which is beneficial in cogging torque reduction.

Meanwhile, slots per pole per phase is given by Equation (1), depicting A Fractional Slot Concentrated Winding (FSCW) configuration with the merits of higher torque production, reduction or minimization of copper losses owing to short end design winding arrangement, and reduced manufacturing complexity. Nonetheless, the phase shift or displacement of the designed five-phase motor is 72 °, as derived from Equation (2).

$$q = \frac{Qs}{2pm} \tag{1}$$

$$\alpha_{ph} = \frac{2\pi}{m} = \frac{360}{5}^{o} \tag{2}$$

Hence, given rise to the sinusoidal current of the five-phase motor under balanced conditions, as presented in Equation (3)

$$\begin{cases} i_A = \mathrm{Im}\cos\omega t \\ i_B = \mathrm{Im}\cos\left(\omega t - 72^{o}\right) \\ i_C = \mathrm{Im}\cos\left(\omega t - 144^{o}\right) \\ i_D = \mathrm{Im}\cos\left(\omega t - 216^{o}\right) \\ i_E = \mathrm{Im}\cos\left(\omega t - 288^{o}\right) \end{cases} \tag{3}$$

Meanwhile, the electrical frequency at the design speed of 1500rpm is given by Equation (4).

$$f = \frac{P\,r\,N}{120} = 237.5Hz \tag{4}$$

Furthermore, the mechanical angle between adjacent stator slots of the motor or the design is determined by Equation (5), while that of the electrically measured angle established between adjacent design slots can be derived from Equation (6). Meanwhile, the star-of-slot winding configuration of both single and double designs is illustrated in Figures 1 (a) and 1(b), respectively.

Nonetheless, the Single-Layer Winding Stator Permanent Magnet Flux-Switching (SWSPMFS) motor and the Double-Layer Winding Stator Permanent Magnet Flux-Switching (DWSPMFS) motor are respectively presented in Figures 2 (a) and 2(b) to substantiate or strengthen the design analysis. Besides, the motor phase identification is demonstrated in Figure 3. To intuitively buttress the aforementioned design analysis, the selected design specifications are presented in Table 1.

$$\alpha_m = \frac{2\pi}{Qs} = 18^{o} \tag{5}$$

$$\alpha_e = \frac{\mathrm{Pr}}{2} \times \alpha_m = 171^{o} \tag{6}$$

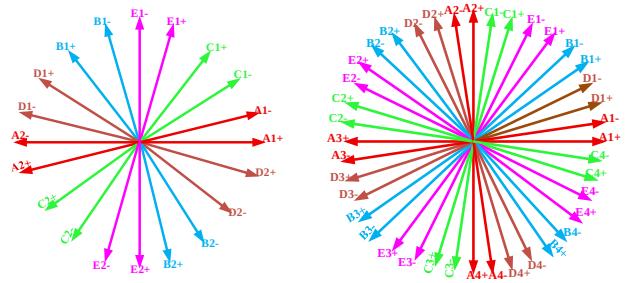

(a) (b)

Fig. 1 Star of slot winding designs: (a) Single-layer, and (b) Double-layer.

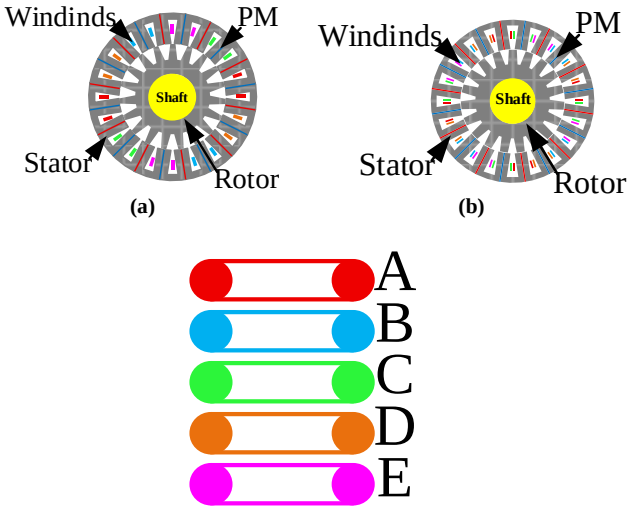

(c)

Fig. 2 Motor design topologies: (a) SWSPMFS motor, (b) DWSPMFS motor, and (c) Phase identifications.

Table 1. Design specifications of both SWSPMFS motor and DWSPMFS motor

Design Specification	SWPMSF Motor	DWSPMFS Motor
Rotor-Stator Pole Synergy	20/19	20/19
PM material	NdFe35	NdFe35
Rotor outer measured diameter (mm)	91.7	91.7
Rotor inner measured diameter (mm)	40	40
Stator outer measured diameter (mm)	145	145
Stator inner measured diameter (mm)	92.7	92.7
Type of laminated iron core material	DW540_50	DW540_50
Rated speed (rev/min)	1500	1500
Axial length (mm)	51.6	51.6
Number of turns	35	35
Airgap length	0.5	0.5
Stator-slots/Rotor-pole number	20/19	20/19
Rated current	8.2	8.2

2.1. Optimization Process and Analysis of both SWSPMFS Motor and DWSPMFS Motor

To achieve an optimal design performance of both the SWSPMFS motor and DWSPMFS motor, the multi-objective parameter optimization methods extensively analyzed in [29-32] are utilized to effectively enhance the optimization process.

Meanwhile, the design parameter model of SPMFS motors considered in this research paper is labeled and presented in Figure 3. Nonetheless, the PM volume is kept the same in both the SWSPMFS motor and DWSPMFS motor to ensure a fair comparative analysis. Furthermore, the design optimization procedure or process is illustrated in Figure 4.

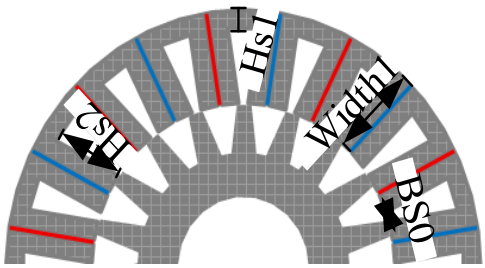

Fig. 3 Design parameter model analysis

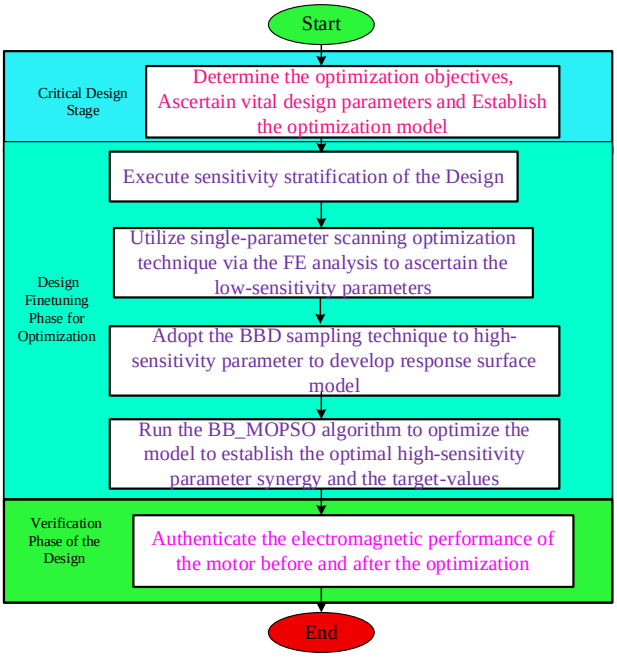

Fig. 4 Design optimization flow chart analysis

2.1.1. Optimization Model Constraints Analysis

To unearth the best and Significant Motor Design Parameters for both the SWSPMFS motor and DWSPMFS motor while aiming at the imperative motor design requirements, the output electromagnetic torque and torque ripple components are selected or adopted as key optimization constraint objectives and are presented in Equation (7). Moreover, Tables 2 and 3 present or report the initial, variation, and optimal design values of both SWSPMFS motor and DWSPMFS motor, respectively. Nonetheless, it can be readily observed that the SWSPMFS motor unveils an average or mean torque of 6.41Nm, with a corresponding ripple torque of 4.98, while that of the DWSPMFS motor exhibits an average torque of 8.35Nm, with a corresponding torque ripple of 4.03. Hence, this demonstrates an average torque increase of 30.27% and a torque ripple reduction of 19.08% in the DWSPMFS motor compared to the SWSPMFS motor.

$$s.t: \begin{Bmatrix} min(zi) \le zi \le max(zi) \\ g1(x) = 6.4 - Tavg \le 0 \\ g2(x) = Trip - 5 \le 0 \end{Bmatrix} \quad (7)$$

Moreover, it is imperative to point out from Table 2 and Table 3 that the SWSPMFS motor exhibits an optimal torque ripple value of 5.04% and an FEA validation value of 4.98%, revealing a minimal difference of 0.06. Nevertheless, the design shows close alignment or agreement, which depicts consistency in the optimization design outcome. Nonetheless, the DWSPMFS motor unearths an optimal torque ripple of 4.08% and FEA validation of 4.03% with an infinitesimal difference of 0.05, depicting a closed design agreement in the optimization design outcome. Hence, unveiling minimal torque ripple in DWSPMFS motor than SWSPMFS motor.

Table 2. Design optimization parameter analysis of SWSPMFS motor

Design Specification	Units	Initial Design Parameter Values	Variation Range Values	Optimal Values of the Design	FEA Authentication
Width 1	mm	26.85	24-28.42	26	26
BS0	mm	3.867	3.6-3.9	3.639	3.639
Hs 1	mm	5.845	5-6	5.2	5.2
Hs 2	mm	22.65	21-23.4	21.51	21.51
Tavg	Nm	5.34	/	6.41	6.41
Trip	%	7.36	/	5.04	4.98
PM Area	mm^2	29.95	/	/	/

Table 3. Design optimization parameter analysis of DWSPMFS motor

Design Specification	Units	Initial Design Parameter Values	Variation Range Values	Optimal Values of the Design	FEA Authentication
Width 1	mm	26.85	24-28.42	26	26
BS0	mm	3.867	3.6-3.9	3.639	3.639
Hs 1	mm	5.845	5-6	5.2	5.2
Hs 2	mm	22.65	21-23.4	21.51	21.51
Tavg	Nm	7.31	/	8.35	8.35
Trip	%	7.85	/	4.08	4.03
PM Area	mm^2	29.95	/	/	/

To intuitively buttress the aforementioned optimization analysis of both the SWSPMFS motor and DWSPMFS motor, the average torque waveforms before (initial) and after the optimization process are illustrated in Figures 5 (a) and 5(b), respectively. Meanwhile, it can be seen that the DWSPMFS motor exhibits higher torque output performance compared to the SWSPMFS motor, which is a merit in EV traction utilization or applications.

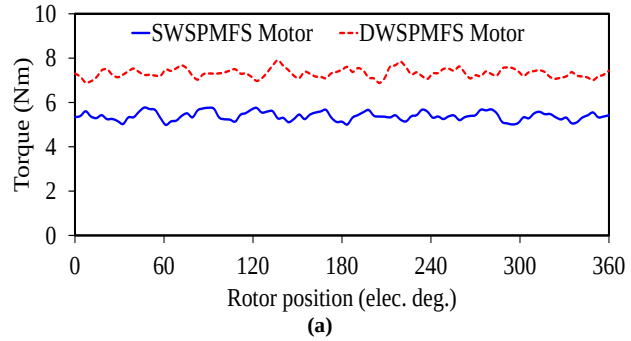

(a)

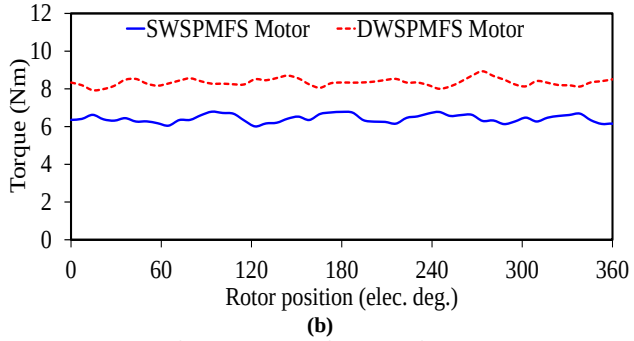

(b)

Fig. 5 Torque waveform analysis before and after design optimization: (a) Before optimization, and (b) After optimization.

3. Results and Discussion

3.1. No-Load Condition Performance Analysis

The no-load motor operating condition analysis section of the paper focused on the no-load Back Electromotive Force (Back-EMF), flux density, flux linkage, and generated cogging torque. Furthermore, it can be observed in Figures 6 (a) and 6(b), respectively, that both the SWSPMFS motor and DWSPMFS motor exhibit a sinusoidal back-EMF, which is key in brushless AC motor operation and desirable in EV traction for ensuring torque ripple or pulsation reduction, vibration and acoustic noise reduction, and reduced mechanical stress of the motor.

Thus, it exhibits smooth electromagnetic torque generation with low torque ripple. Moreover, as illustrated in Figure 6(b), the DWSPMFS motor exhibits a higher back-EMF, which is beneficial for torque production compared to the SWSPMFS motor shown in Figure 6(a).

Moreover, Figure 7 illustrates the harmonic-order waveform of the Back-EMF of both the SWSPMFS motor and DWSPMFS motor topologies. Furthermore, it can be observed that the 9th, 11th, 19th, and 21st orders of harmonics, which are factors responsible for causing or inducing torque pulsations in five-phase configured motors, are higher in the DWSPMFS motor compared to the SWSPMFS motor. Also, the Total Harmonic Distortion (THD) exhibited by the SWSPMFS motor is 1.69%, while that of the DWSPMFS motor is 19.37%. Meanwhile, the computation of the THD can be derived from Equation (8).

$$THD = \frac{\sqrt{\sum_{z=2,\ldots}^{\infty} {E_{bz}}^2}}{E_{b1}} \quad (8)$$

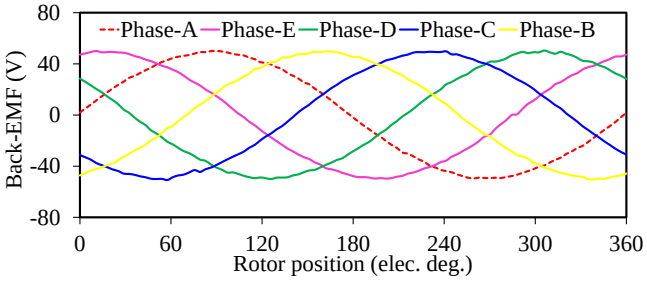

Fig. 6 Back-EMF waveform analysis of SWSPMFS motor and DWSPMFS motor: (a) SWSPMFS motor, and (b) DWSPMFS motor.

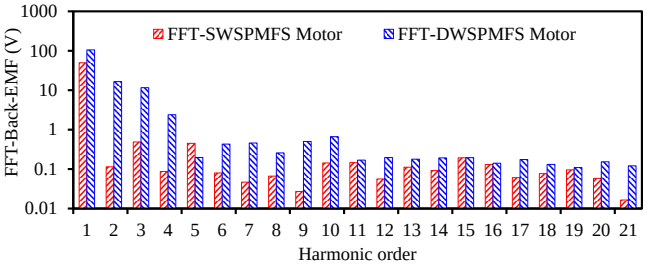

Fig. 7 Back-EMF harmonic-order analysis of SWSPMFS motor and DWSPMFS motor

Furthermore, Figures 8(a) and 8(b) depict the flux linkage of both the SWSPMFS motor and DWSPMFS motor, respectively. Meanwhile, as highlighted in Figure 8(b), the DWSPMFS motor exhibits a higher flux linkage, which suggests a potentially strong magnetic coupling and a corresponding high torque compared to the SWSPMFS motor in Figure 8(a). Moreover, the magnetic field or flux distribution of both the SWSPMFS motor and DWSPMFS motor is presented in Figures 9(a) and 9(b), chronologically or respectively. Also, it can be seen or recognized that the DWSPMFS motor in Figure 9(b) exhibits a more concentrated flux distribution, which is beneficial for torque production enhancement compared to the SWSPMFS motor in Figure 9 (a), indicating a slight leakage of flux away from the air gap. Nonetheless, the flux density distribution of both the SWSPMFS motor and DWSPMFS motor is illustrated in Figures 10(a) and 10(b), respectively, with the SWSPMFS motor in Figure 10(a) exhibiting the same or comparable flux density compared to the DWSPMFS motor in Figure 10(b). Thus, exhibiting the same overload capacity for both the DWSPMFS motor and the SWSPMFS motor.

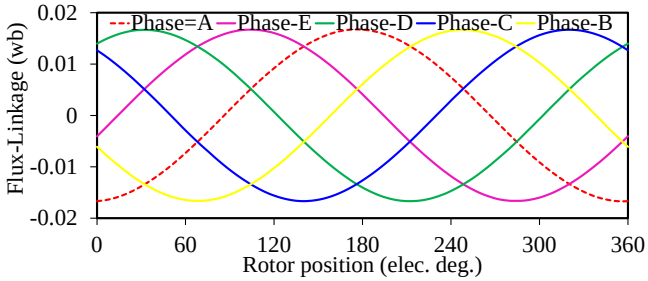

Fig. 8 Flux-Linkage waveform analysis of both SWSPMFS motor and DWSPMFS motor: (a) SWSPMFS motor, and (b) DWSPMFS motor.

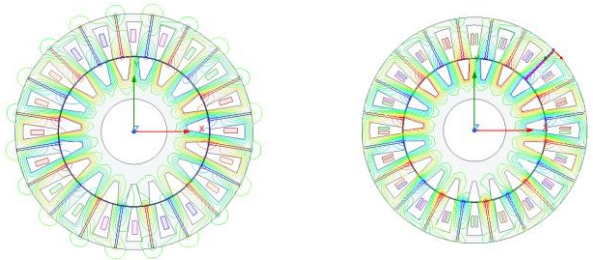

Fig. 9 Magnetic flux-distribution analysis of SWSPMFS motor and DWSPMFS motor: (a) SWSPMFS motor, and (b) DWSPMFS motor.

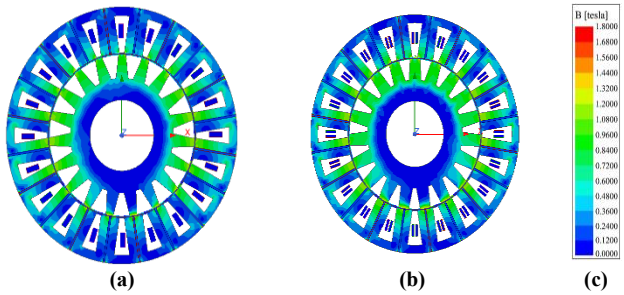

Fig. 10 Flux density analysis of SWSPMFS motor and DWSPMFS motor

Furthermore, the radial and tangential measured flux density of both the SWSPMFS motor and DWSPMFS motor are illustrated in Figures 11(a) and 11(b), respectively. Meanwhile, it can be established or observed intuitively that both motors exhibit comparable radial and tangential flux densities, with feasible or potential to contribute to torque production enhancement with reduced torque ripple, which is key in EV traction applications.

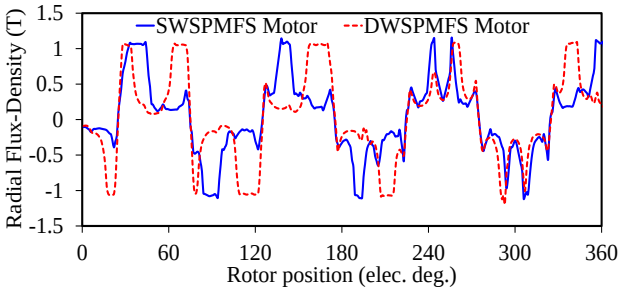

(a)

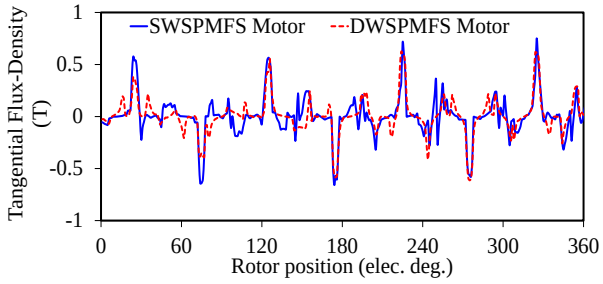

(b)

Fig. 11 Radial and tangential flux density of both SWSPMFS motor and DWSPMFS motor: (a) Radial flux density, and (b) Tangential flux density.

The cogging torque, which can be defined as unwanted periodic torque generated or produced in permanent magnet-designed electric motors owing to the interruption between the established or generated magnetic field of the configured rotor and the laminated stator teeth, especially or even when there is no current supplied or injected into the stator-configured windings, is critical in applications such as EVs and equivalent high-performance applications.

Meanwhile, the cogging torque of both the SWSPMFS and DWSPMFS motors is shown in Figure 12. Moreover, the SWSPMFS motor unveils a cogging torque is 0.33 Nm, and that of DWSPMFS motor exhibits a cogging torque of 0.29 Nm, demonstrating a 12.12% cogging torque reduction in the DWSPMFS motor.

Hence, it benefits from smooth rotation, reduced vibration and acoustic noise, with better or enhanced low-speed performance compared to the SWSPMFS motor.

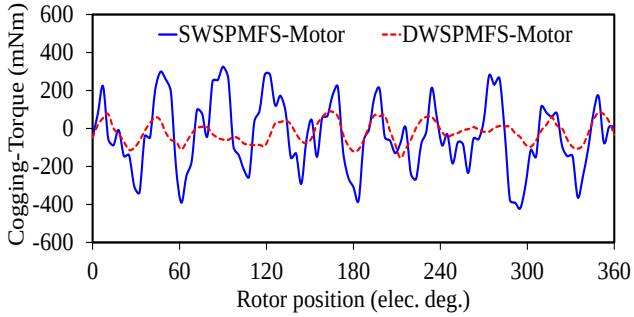

Fig. 12 Cogging torque analysis of both SWSPMFS motor and DWSPMFS motor

3.1.1. Design Load Analysis of both SWSPMFS Motor and DWSPMFS Motor

The torque analysis of both the SWSPMFS motor and the DWSPMFS motor based on various current angles is presented in Figure 13. Moreover, it can be observed that the DWSPMFS motor consistently exhibits a higher output torque compared to the SWSPMFS motor.

Besides, to ensure intuitive and quantitative analysis of the aforementioned designs, the DWSPMFS motor exhibits 8.35 Nm at an angle of 0°, while the SWSPMFS motor exhibits 6.41 Nm at the same angle of 0°, depicting a 30.27% increase in torque production in the DWSPMFS motor compared to the SWSPMFS motor.

Nonetheless, the torque ripple measured at distinct current angle conditions for both the SWSPMFS motor and DWSPMFS motor is illustrated in Figure 14. Meanwhile, it can be seen that the DWSPMFS motor consistently exhibits a minimal torque ripple compared to the SWSPMFS motor.

Besides, to quantitatively buttress the analysis, the DWSPMFS motor exhibits a generated torque ripple of 4.03%, while that of the SWSPMFS motor exhibits a torque ripple of 4.98%, depicting a 19.08% reduction in torque ripple in the DWSPMFS motor topology compared to the SWSPMFS motor. Nonetheless, the percentage torque ripple can be derived from Equation (9).

$$\%T_{rip} = \frac{T_{pek-pek}}{T_{avg}} \times 100\% \quad (9)$$

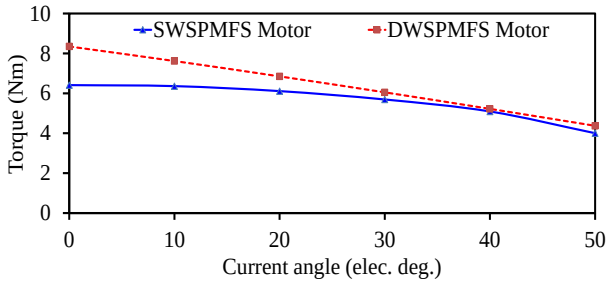

Fig. 13 Torque angle analysis of both SWSPMFS motor and DWSPMFS motor

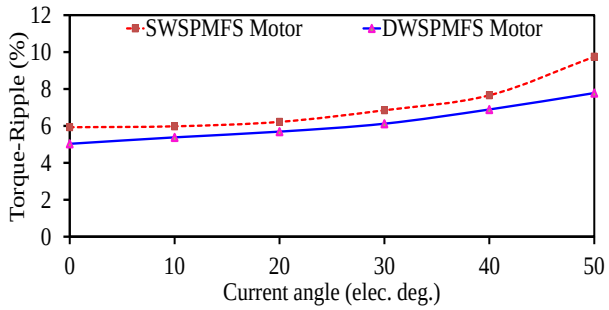

Fig. 14 Torque ripple analysis of both SWSPMFS motor and DWSPMFS motor at various current angles

3.1.2. Design Losses and Efficiency Analysis of SWSPMFS Motor and DWSPMFS Motor

The efficiency of an electrically designed motor is one of the critical components, if not the core, in determining how effectively and comprehensively the motor converts the electrical energy supply to the rotational or mechanical output energy. Hence, the rotor, Permanent Magnet (PM), and stator losses of both the SWSPMFS motor and DWSPMFS motor are presented in Figures 15 (a)-(c), respectively. As presented in Figure 15(a), the rotor losses at angles of 0º, 10º, and 20º are higher in the SWSPMFS motor compared to the DWSPMFS motor. Nonetheless, it is imperative or significant factor to highlight that the rotor losses at the angles of 30º, 40º, and 50º in the DWSPMFS motor are higher compared to the SWSPMFS motor.

Furthermore, the PM losses analysis, as illustrated intuitively in Figure 15(b), it is significant to highlights that the DWSPMFS motor exhibits higher PM losses at all the distinct current angle conditions compared to the SWSPMFS motor. Moreover, as demonstrated in Figure 15(c), the Stator losses at angles of 0º, 20º, and 40 ° are higher in the SWSPMFS motor. Besides, it is equally important to highlight or underscore that the stator losses at an angle 30º and 50º are higher in the DWSPMFS motor compared to the SWSPMFS motor.

Although it can be deduced from the aforementioned analysis that the DWSPMFS motor unveils a higher loss in some cases compared to the SWSPMFS motor, thanks to the higher electromagnetic output torque exhibited by the DWSPMFS motor, it exhibits higher efficiency at the current angle of 0 ° compared to the SWSPMFS motor, as illustrated in Figure 16. To further substantiate the aforementioned analysis, the DWSPMFS motor exhibits an efficiency of 93.98% at an angle of 0º, while that of SWSPMFS motor unveils an efficiency of 92.1% at the same angle of 0 °. Hence, depicting 2.04% efficiency increase in the DWSPMFS motor, which demonstrates better energy conversion compared to the SWSPMFS motor. Also, the percentage design efficiency can be derived from Equation (10).

$$\%_{\eta} = \frac{(T_{avg\omega})}{(T_{avg\omega})+P_{cu}+P_{pm}+P_{rt}+P_{st}} \times 100\% \qquad (10)$$

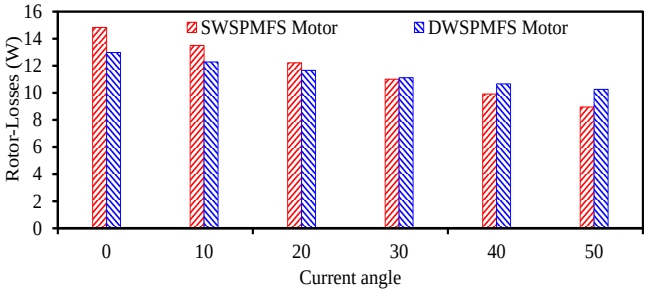

(a)

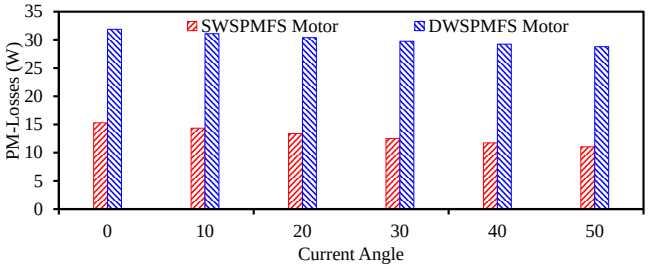

(b)

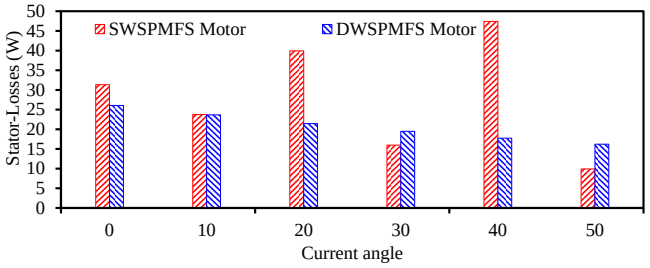

(c)

Fig. 15 Design losses analysis of SWSPMFS motor and DWSPMFS Motor (a) Rotor losses, (b) PM losses, and (c) Stator losses.

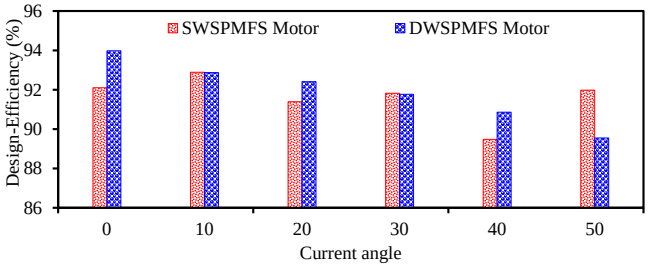

Fig. 16 Design efficiency analysis of SWSPMFS motor and DWSPMFS motor

3.1.3. Magnetic Phase Isolation Analysis of SWSPMFS Motor and DWSPMFS Motor

Magnetic phase isolation can be defined as the degree to which the established magnetic field of one phase is concentrated within its own formed magnetic loop, limiting interaction with other phases and minimizing mutual coupling. Since this analysis is imperative to ensure reliable and fault-tolerant motor operation for critical applications such as EV traction, the self and mutual inductances of both the SWSPMFS motor and the DWSPMFS motor are presented in Figures 17(a) and 17(b), respectively. Nonetheless, it can be observed in Figure 17(b) that the DWSPMFS motor demonstrates a higher measured self-inductance, which is a merit for limiting a high short-circuit current or rapid change in current, and a lower or minimal mutual inductance, which is a merit of better magnetic phase isolation in case of fault conditions compared to the SWSPMFS motor in Figure 17(a). Hence, this reveals that the DWSPMFS motor exhibits a higher potential for fault-tolerant operation compared to the SWSPMFS motor. Moreover, it is imperative to emphasize that the units of the inductance are in mH.

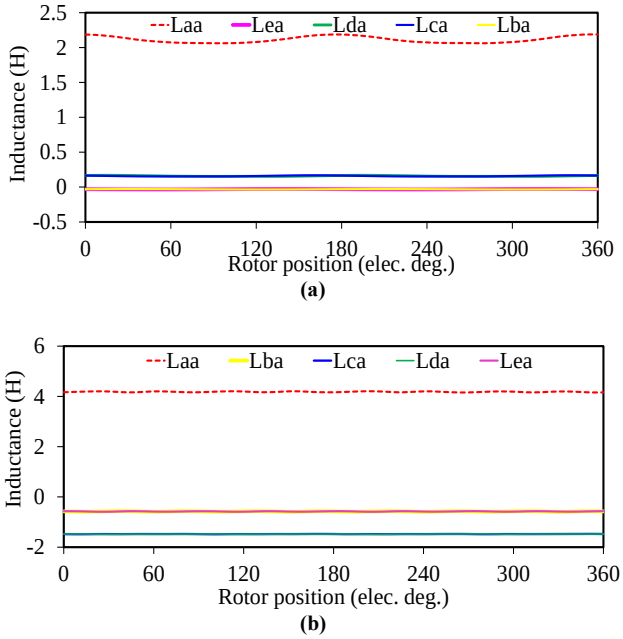

Fig. 17 Magnetic phase isolation analysis (a) Self and mutual inductance of SWSPMFS motor, and (b) Self and mutual inductance of DWSPMFS motor.

4. Conclusion

The SWSPMFS motor and DWSPMFS motor with 20/19 rotor-stator pole synergy, which have not been simultaneously designed, modeled, optimized, analyzed, and compared extensively with the same selected design parameters and dimensions in current or existing literature, leaving a research gap, have been comprehensively and successfully analyzed in this research work. The multi-optimization technique was employed via the Ansys Maxwell Electromagnetic software to unveil which of these aforementioned designed motors is suitable for EV traction drive or propulsion applications based on characteristics such as output torque, cogging torque, torque ripple, efficiency, and fault-tolerant capability. Moreover, the SWSPMFS motor topology unveiled an average torque output of 6.41 Nm, while that of the DWSPMFS motor exhibited an average torque output of 8.35 Nm. Hence, demonstrating a 30.27% increase in the DWSPMFS motor compared to the SWSPMFS motor. Nonetheless, the torque ripple exhibited by the SWSPMFS motor is 4.98%, while that of the DWSPMFS motor is 4.03, which demonstrates a torque ripple reduction of 19.08% in the DWSPMFS motor.

Besides, it is imperative to highlight that the cogging torque generated by the SWSPMFS motor is 0.33 Nm, while that generated by the DWSPMFS motor is 0.29, which demonstrates a cogging torque reduction of 12.12% in the DWSPMFS motor. Furthermore, the efficiency obtained by the SWSPMFS motor is 92.1%, while the DWSPMFS motor exhibited an efficiency of 93.98%, which depicts an increase of 2.04% in the DWSPMFS motor compared to the SWSPMFS motor.

Moreover, it is equally significant to highlight that the DWSPMFS motor unveils the highest THD of 19.37% compared to the SWSPMFS motor, with a significant decrease of 1.69%. Nevertheless, it is imperative to emphasize, from the aforementioned analysis of the achieved results, that the DWSPMFS motor is a suitable potential motor design candidate for EV traction application with better fault-tolerant operating capacity compared to the SWSPMFS motor topology.

Although the differences established between the optimal torque ripple value and FEA torque ripple validation value are acceptable from an optimization and motor engineering point of view, it is imperative to be considered or investigated in future research.

References

[1] Mahmoud S.R. Saeed, and Essam E.M. Mohamed, "Partitioned Topologies of Switched Flux Permanent Magnet Machines for Electric Vehicles," *International Journal of Computer Applications*, vol. 179, no. 41, pp. 23-30, 2018. [CrossRef] [Google Scholar]

[2] Arigela Satya Veerendra, Mohd Rusllim Bin Mohamed, and Fausto Pedro García Márquez, "Energy Management Control Strategies for Energy Storage Systems of Hybrid Electric Vehicle: A Review," *Energy Storage*, vol. 6, no. 1, pp. 1-24, 2024. [CrossRef] [Google Scholar] [Publisher Link]

[3] Jawad Faiz, and Majid Maktobian, "Performance Enhancement of Flux Switching Motor for Electric Vehicle Applications: An Overview," *IET Electrical Systems in Transportation*, vol. 2024, no. 1, pp. 1-22, 2024. [CrossRef] [Google Scholar] [Publisher Link]

[4] Wei Hua et al., "A Novel Rotor-Permanent Magnet Flux-Switching Machine," *2015 Tenth International Conference on Ecological Vehicles and Renewable Energies*, Monte Carlo, Monaco, pp. 1-10, 2015. [CrossRef] [Google Scholar] [Publisher Link]

[5] Iain Urquhart et al., "Mechanically Actuated Variable Flux IPMSM for EV and HEV Applications," *2013 World Electric Vehicle Symposium and Exhibition*, Barcelona, Spain, pp. 1-12, 2013. [CrossRef] [Google Scholar] [Publisher Link]

[6] Ruiwu Cao, Chris Mi, and Ming Cheng, "Quantitative Comparison of Flux-Switching Permanent-Magnet Motors with Interior Permanent Magnet Motor for EV, HEV, and PHEV Applications," *IEEE Transactions on Magnetics*, vol. 48, no. 8, pp. 2374-2384, 2012. [CrossRef] [Google Scholar] [Publisher Link]

[7] Ming Cheng et al., "Overview of Stator-Permanent Magnet Brushless Machines," *IEEE Transactions on Industrial Electronics*, vol. 58, no. 11, pp. 5087-5101, 2011. [CrossRef] [Google Scholar] [Publisher Link]

[8] Yanjian Zhou, and Z.Q. Zhu, "Torque Density and Magnet usage Efficiency Enhancement of Sandwiched Switched Flux Permanent Magnet Machines using V-Shaped Magnets," *IEEE Transactions on Magnetics*, vol. 49, no. 7, pp. 3834-3837, 2013. [CrossRef] [Google Scholar] [Publisher Link]

[9] Zegang Xu, Shaojun Xie, and Peng Mao, "Analytical Design of Flux-Switching Hybrid Excitation Machine by a Nonlinear Magnetic Circuit Method," *IEEE Transactions on Magnetics*, vol. 49, no. 6, pp. 3002-3008, 2013. [CrossRef] [Google Scholar] [Publisher Link]

[10] Xiaohong Xue et al., "Design of Five-Phase Modular Flux-Switching Permanent-Magnet Machines for High Reliability Applications," *IEEE Transactions on Magnetics*, vol. 49, no. 7, pp. 3941-3944, 2013. [CrossRef] [Google Scholar] [Publisher Link]

[11] Christian Sanabria-Walter, Henk Polinder, and Jan Abraham Ferreira, "High-Torque-Density High-Efficiency Flux-Switching PM Machine for Aerospace Applications," *IEEE Journal of Emerging and Selected Topics in Power Electronics*, vol. 1, no. 4, pp. 327-336, 2013. [CrossRef] [Google Scholar] [Publisher Link]

[12] Wei Hua et al., "Analysis of Two Novel Five-Phase Hybrid-Excitation Flux-Switching Machines for Electric Vehicles," *IEEE Transactions on Magnetics*, vol. 50, no. 11, pp. 1-5, 2014. [CrossRef] [Google Scholar] [Publisher Link]

[13] Wei Hua et al., "Electromagnetic Performance Analysis of Hybrid-Excited Flux-Switching Machines by a Nonlinear Magnetic Network Model," *IEEE Transactions on Magnetics*, vol. 47, no. 10, pp. 3216-3219, 2011. [CrossRef] [Google Scholar] [Publisher Link]

[14] Feng Li et al., "Analysis of Fault Tolerant Control for a Nine-Phase Flux-Switching Permanent Magnet Machine," *IEEE Transactions on Magnetics*, vol. 50, no. 11, pp. 1-4, 2014. [CrossRef] [Google Scholar] [Publisher Link]

[15] Mohd Firdaus Mohd Ab Halim, Erwan Sulaiman, and R.N.F.K.R. Othman, "Flux Switching Machine: Design Variation Review," *International Journal of Advanced Trends in Computer Science and Engineering*, vol. 9, no. 2, pp. 2422-2430, 2020. [CrossRef] [Google Scholar] [Publisher Link]

[16] Amin Nobahari, Mehdi Aliahmadi, and Jawad Faiz, "Performance Modifications and Design Aspects of Rotating Flux Switching Permanent Magnet Machines: A Review," *IET Electric Power Applications*, vol. 14, no. 1, pp. 1-15, 2020. [CrossRef] [Google Scholar] [Publisher Link]

[17] Shichao Ning et al., "A Novel Double Stator Hybrid-Excited Halbach Permanent Magnet Flux-Switching Machine For EV/HEV Traction Applications," *Scientific Reports*, vol. 14, no. 1, pp. 1-19, 2024. [CrossRef] [Google Scholar] [Publisher Link]

[18] Hamid Ebrahimi, Hossein Torkaman, and Hamid Javadi, "Simultaneous Improvement of Cogging Torque and Torque Density in Axial Flux-Switching Permanent Magnet Motor," *IET Electric Power Applications*, vol. 18, no. 3, pp. 312-324, 2024. [CrossRef] [Google Scholar] [Publisher Link]

[19] Xiaozhuo Xu et al., "Performance Analysis and Optimization of Permanent Magnet Flux Switched Linear Motor for Ropeless Elevator," *IET Electric Power Applications*, vol. 17, no. 1, pp. 47-57, 2023. [CrossRef] [Google Scholar] [Publisher Link]

[20] Hossein Torkaman, Aghil Ghaheri, and Ali Keyhani, "Axial Flux Switched Reluctance Machines: A Comprehensive Review of Design and Topologies," *IET Electric Power Applications*, vol. 13, no. 3, pp. 310-321, 2019. [CrossRef] [Google Scholar] [Publisher Link]

[21] Hossein Torkaman, Aghil Ghaheri, and Ali Keyhani, "Design of Rotor Excited Axial Flux-Switching Permanent Magnet Machine," *IEEE Transactions on Energy Conversion*, vol. 33, no. 3, pp. 1175-1183, 2018. [CrossRef] [Google Scholar] [Publisher Link]

[22] Bingchang Lv et al., "Performance Analysis of Asymmetrical Less-Rare-Earth Permanent Magnet Motor for Electric Vehicle," *IET Electrical Systems in Transportation*, vol. 12, no. 1, pp. 36-48, 2022. [CrossRef] [Google Scholar] [Publisher Link]

[23] Monika Verma, Madhusudan Singh, and Mini Sreejeth, "Integrated Taguchi Method-Assisted Polynomial Metamodelling and Genetic Algorithm based Optimisation of a Surface Inset Permanent Synchronous Motor for Performance Improvement," *IET Electrical Systems in Transportation*, vol. 12, no. 1, pp. 26-35, 2021. [CrossRef] [Google Scholar] [Publisher Link]

[24] Aghil Ghaheri, Ebrahim Afjei, and Hossein Torkaman, "A Novel Axial Air-Gap Transverse Flux Switching PM Generator: Design, Simulation and Prototyping," *IET Electric Power Applications*, vol. 17, no. 4, pp. 452-463, 2023. [CrossRef] [Google Scholar] [Publisher Link]

[25] Sadjad Shafiei et al., "A Modified Partitioned-Stator Flux-Switching Permanent Magnet Machine for Enhancing Torque-Density in Electric Vehicle Powertrains," *IET Electric Power Applications*, vol. 19, no. 1, pp. 1-20, 2025. [CrossRef] [Google Scholar] [Publisher Link]

[26] Xiaoyong Zhu et al., "Torque Component Redistribution and Enhancement for Hybrid Permanent Magnet Motor with Permanent Magnet Offset Placement," *IEEE Transactions on Transportation Electrification*, vol. 9, no. 1, pp. 631-641, 2023. [CrossRef] [Google Scholar] [Publisher Link]

[27] Luca Cinti et al., "Hybrid Excited Permanent Magnet Motor: Analytical Sizing, Finite Element Analysis and Tests," *IEEE Transactions on Industry Applications*, vol. 59, no. 6, pp. 6645-6654, 2023. [CrossRef] [Google Scholar] [Publisher Link]

[28] J.T. Chen, and Z.Q. Zhu, "Winding Configurations and Optimal Stator and Rotor Pole Combination of Flux-Switching PM Brushless AC Machines," *IEEE Transactions on Energy Conversion*, vol. 25, no. 2, pp. 293-302, 2010. [CrossRef] [Google Scholar] [Publisher Link]

[29] Guohai Liu et al., "Multiobjective Deterministic and Robust Optimization Design of a New Spoke-Type Permanent Magnet Machine for the Improvement of Torque Performance," *IEEE Transactions on Industrial Electronics*, vol. 67, no. 12, pp. 10202-10212, 2020. [CrossRef] [Google Scholar] [Publisher Link]

[30] Gang Lei et al., "Techniques for Multilevel Design Optimization of Permanent Magnet Motors," *IEEE Transactions on Energy Conversion*, vol. 30, no. 4, pp. 1574-1584, 2015. [CrossRef] [Google Scholar] [Publisher Link]

[31] Wenxiang Zhao et al., "Multiobjective Optimization of a Double-Side Linear Vernier PM Motor using Response Surface Method and Differential Evolution," *IEEE Transactions on Industrial Electronics*, vol. 67, no. 1, pp. 80-90, 2020. [CrossRef] [Google Scholar] [Publisher Link]

[32] Xiaodong Sun et al., "Multi-Objective Design Optimization of an IPMSM based on Multilevel Strategy," *IEEE Transactions on Industrial Electronics*, vol. 68, no. 1, pp. 139-148, 2021. [CrossRef] [Google Scholar] [Publisher Link]